Journal of Nuclear Materials 405 (2010) 83–94

Contents lists available at ScienceDirect

Journal of Nuclear Materials

journal homepage: www.elsevier.com/locate/jnucmat

Modelling of the effect of dislocation channel on intergranular microcrack nucleation in pre-irradiated austenitic stainless steels during low strain rate tensile loading

Pierre Evrard, Maxime Sauzay *

DMN-SRMA-LC2M, CEA Saclay, 91191 Gif-sur-Yvette, France

ARTICLE INFO

Article history:
Received 8 January 2010
Accepted 3 June 2010

ABSTRACT

In the present article, the effect of dislocation channel on intergranular microcrack nucleation during the tensile deformation of pre-irradiated austenitic stainless steels is studied. Because several slip planes are activated within the dislocation channel, the simple dislocation pile-up model seems not well suited to predict grain boundary stress field. Finite element computations, using crystal plasticity laws and meshes including a channel of finite thickness, are also performed in order to study the effect of some microstructural characteristics on grain boundary stress field. Numerical results show that: the thickness and the length of the dislocation channel influence strongly the grain boundary normal stress field. The grain boundary orientation with respect the stress axis does not affect so much the grain boundary normal stresses close to the dislocation channel. On the contrary far away the dislocation channel, the grain boundary stress field depends on the grain boundary orientation. Based on these numerical results, an analytical model is proposed to predict grain boundary stress fields. It is valuable for large ranges of dislocation channel thickness, length as well as applied stress. Then, a macroscopic microcrack nucleation criterion is deduced based on the elastic–brittle Griffith model. The proposed criterion predicts correctly the influence of grain boundary characteristics (low-angle boundaries (LABs), non-coincident site lattice (non-CSL) high-angle boundaries (HABs), special grain boundaries (GBs)) on intergranular microcrack nucleation and the macroscopic tensile stress required for grain boundary microcrack nucleation for pre-irradiated austenitic stainless steels deformed in argon environment. The criterion based on a dislocation pile-up model (Smith and Barnby) underestimates strongly the nucleation stress. These results confirm that pile-up models are not well suited to predict microcrack nucleation stress in the case of dislocation channels impacting grain boundary. The proposed criterion is applied to the prediction of the IASCC macroscopic nucleation stress for pre-irradiated material tested in PWR environment and the predictions are discussed with respect to experimental data. Finally, the limitations of the continuum modelling are discussed.

1. Introduction

In order to keep the integrity of pressurized water reactors (PWR), it is necessary to understand and predict the failure of core internals. In particular, it is well known that PWR environment and irradiation could lead to in premature failure of some components [1]. PWR environment combined with mechanical loading (temperature 300–340 °C, dissolved hydrogen 30 cm^3/kg, dissolved oxygen <5 ppb, pH = 6.9) can lead to intergranular stress corrosion cracking (IGSCC). Irradiation, modifying the mechanical properties and grain boundary chemistry of materials can assist the IGSCC. This phenomenon is named irradiation assisted stress corrosion cracking (IASCC).

Several authors [2–7] have performed tensile tests in argon, air or PWR environment on austenitic stainless steels previously irradiated to different doses. In comparison with the stress–strain curves of an unirradiated austenitic stainless steel, it has been observed that if the dose increases, the yield stress increases whatever the irradiation temperature [8], the strain rate [9] and the test temperature [10]. From about 10 dpa, the yield stress saturates and reaches 800–1200 MPa [5] for an austenitic stainless steel irradiated and tested at about 350 °C and at strain rate of 3×10^{-4} s^{-1}. The microstructure evolution induced by irradiation has been studied from TEM observations. During irradiation, defects appear such as Frank loops, cavities, black dot and limit dislocation mobility during post-irradiation tensile tests. Consequently, the yield stress increases. However, during post-irradiation tensile tests, regions without defects can appear, named dislocation channel, where the plastic deformation is mainly localized and can reach about

* Corresponding author.
E-mail address: maxime.sauzay@cea.fr (M. Sauzay).

0022-3115/$ - see front matter © 2010 Elsevier B.V. All rights reserved.
doi:10.1016/j.jnucmat.2010.06.006

100–200% [11,12]. Usually, the dislocations channels are observed during slow strain rate tests ($\approx 10^{-8}\ s^{-1}$) carried out at a temperature of about 300 °C [13,7]. For the irradiated materials tested at fast strain rate ($\approx 10^{-3}\ s^{-1}$), at room temperature and low doses, twins are more generally observed [13,7]. Recently, the formation of the dislocation channel has been discussed by Osetsky et al. and Nogaret et al. [14,15] from molecular dynamics and dislocation dynamics computations. In metallic materials similar to austenitic stainless steels, the mechanism proposed is the absorption of Frank loops as helical turns on screw dislocation. Dislocation jogs are formed, which are transported along the screw dislocation lines. Finally, the dislocations are re-emitted in a glide plane different from the initial ones because of cross-slip. This leads to the progressive clearing of the dislocation channel.

Intergranular failure of specimens is generally observed in irradiated austenitic stainless steels tested in PWR environment at slow strain rate or constant stress during the first phase of failure near the free surface, while ductile-dimple fracture zones, at the centre of specimens, are formed during the final phase [13]. For austenitic stainless steels tested in a PWR environment, experimental results have shown that if the irradiation dose and the dissolved hydrogen (DH) concentration increases, then the percentage of intergranular failure increases up to reach 100% at about 30 dpa [16,17]. But, environment effect is not always required. Indeed [13,16,7] observed IG failure in pre-irradiated austenitic stainless steels, irradiated to about 30 dpa and tested in argon environment. In these experiments the percentage of intergranular cracking is about 20%. Furthermore, recent studies have shown that the IASCC failure stress, for an austenitic stainless steel tested in PWR environment decreases with increasing doses [18,17]. Jiao and Was [19] studied the role of dislocation channel on intergranular microcrack nucleation in austenitic stainless steel from TEM observations. The authors have tested an austenitic stainless steel with low staking fault energy (SFE) in PWR environment previously irradiated to 5 dpa at 360 °C. The results show intergranular microcrack nucleation at the intersection between dislocation channel and grain boundaries (channel-GB). Furthermore [20] show that localized deformation bands promote strongly the IGSCC. Consequently, it seems that dislocation channel plays a key-role in intergranular microcrack nucleation.

Dislocation channel is generally modelled using the dislocation pile-up theory [11,7]. However, several slip planes are activated within the dislocation channel [21,22]. Consequently, the dislocation pile-up models do not seem well suited to predict the GB stress field. In the present study, a large number of finite element (FE) computations, using crystal elastic–plasticity laws, are performed and the stress fields at the GB are studied. The influence of some microstructural characteristics on grain boundary stress fields is studied: dislocation channel thickness, length and GB orientation in relation to the tensile axis. An analytical model for computing easily the GB stress field is deduced. A microcrack nucleation criterion is formulated and is discussed in relation with some experimental data. Finally, the assumptions made are discussed and the limitations of the continuum modelling are underlined.

2. FE meshes of microstructures and constitutive laws

To study the influence of the dislocation channel thickness and length on GB stress fields, a first numerical microstructure, named M1, (Fig. 1) has been generated using the FE software Cast3m [23]. A dislocation channel, defined by the thickness '*t*', the length '*L*', inclined to 45° with respect the tensile axis and surrounded by a grain, has been generated. Grain and dislocation channels are surrounded by a matrix. The GB normal is inclined to $\alpha = 35°$ with

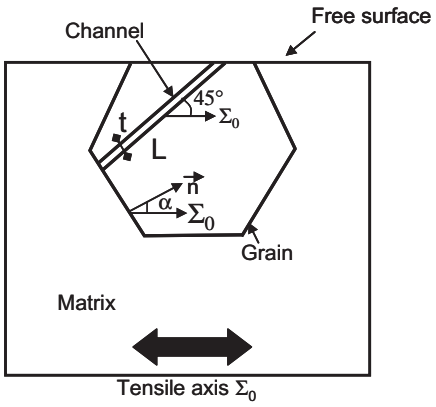

Fig. 1. Microstructure M1 generated using the FE software Cast3m ($\alpha = 35°$).

respect the tensile axis. In order to maximize the strain localization, the dislocation channel comes out toward a free surface. To study the influence of the angle α, a second microstructure, named M2, has been generated (Fig. 2) for which the angle between the GB normal and the tensile axis is $\alpha = 0°$. The microstructures are subjected to a tensile load, Σ_0, such as defined in Figs. 1 and 2. Boundary conditions are applied in order to have a pure tension test and a plane strain problem.

As the pile-up model [24], the stress field at the intersection (pile-up or channel)-GB can be written as $\Sigma = f(r)g(\theta)$ with (r, θ) the polar coordinate. Then, at the intersection channel-GB, a radial mesh has been generated (Fig. 3). The mesh has been extruded in the third direction and a 3D numerical microstructure is therefore obtained. The influence of the mesh size has been studied in details and no influence has been observed on GB normal stress field if the mesh size is small enough. In order to have a better estimation of the GB stresses near the dislocation channel and limited time computation, a 5 nm mesh size has been chosen for GB discretization. The same mesh size has been used for all meshed microstructures. Finally, the influence of the time step has been studied and there is not influence on the GB stresses computations if it is enough small. In the following, the GB stress fields will be plotted in function of the variable '*r*' such as defined in Fig. 3.

To model the mechanical behaviour of the dislocation channel, the anisotropy Kocks crystal viscoplasticity law [25,26] has been used applied to FCC crystal (12 slip systems [1 1 1], {1 1 0}). This law has been implemented in the software Cast3m using a subroutine UMAT which has already used in [27]. The shear strain on each slip system (s) is computed by a viscoplastic flow law:

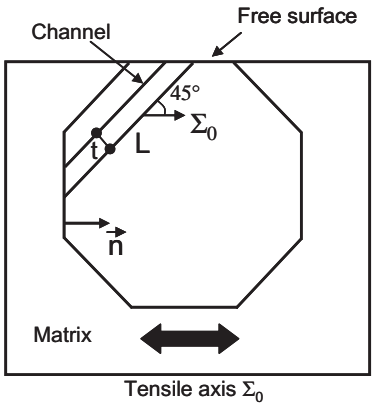

Fig. 2. Microstructure M2 generated using the FE software Cast3m ($\alpha = 0°$).

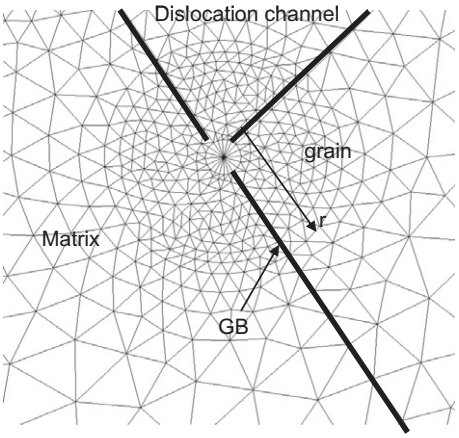

Fig. 3. Radial mesh generated at the intersection between dislocation channelling and GB.

$$\dot{\gamma}_{vp}^{(s)} = A \sinh\left(\frac{\tau^{(s)}}{\tau_c^{(s)}}\right)^{\frac{1}{m}} sign(\tau^{(s)}) \quad (1)$$

if $\tau^{(s)} \geqslant \tau_0 + \tau_c^{(s)}$ otherwise $\dot{\gamma}_{vp}^{(s)} = 0$. $\tau^{(s)}$ is the shear stress on each slip system (s), A and m are two parameters accounting for viscosity effects. The hardening on each slip system (s) is computed by:

$$\dot{\tau}_c^{(s)} = \sum_{u=1}^{u=12} h^{(s)u} \dot{\gamma}^u \quad (2)$$

with $h^{(s)u} = H^{(s)}$ if $(s) = u$ and $h^{(s)u} = qH^{(s)}$ if $(s) \neq u$. $H^{(s)}$ is obtained by the following expressions:

$$H^{(s)} = h_0 \left(\frac{\tau_{sat} - \tau_c^{(s)}}{\tau_{sat} - \tau_0}\right) sign(\tau_{sat} - \tau_0) \quad \tau_{sat} = \bar{\tau}\left(\frac{\sum_{s=1}^{s=12} \dot{\gamma}^{(s)}}{A}\right)^n \quad (3)$$

q, h_0, $\bar{\tau}$ are respectively the latent hardening, the coefficient hardening, and the stress controlling saturation. The elastic behaviour is model by a cubic elasticity at 300 °C, C_{11} = 178 GPa, C_{12} = 125 GPa and C_{44} = 81 GPa (anisotropy coefficient $a = 2C_{44}/(C_{11} - C_{12}) = 3.05$ [28,29]). The crystallographic orientation of the dislocation channel is chosen in order to have a well-oriented dislocation channel (Schmid factor of 0.5). SEM micrographs show that no plasticity is observed apart from the dislocation channel [20]. Furthermore, TEM micrographs show that the dislocation density, measured after high-dose irradiation (10 dpa, 320 °C) is so low ($<10^{11}$ m^{-2}) that close to the channel-GB intersection, no mobile dislocation is available [30]. Consequently, we used elastic law to model the behaviour of the grain and the matrix surrounding the dislocation channel. Furthermore, in this first study an isotropic elastic law is used in order to simplify the model. For an austenitic stainless steel at 300 °C, Young modulus and Poisson ratio are respectively E = 180 GPa and ν = 0.3.

The tensile strain–stress curves performed on pre-irradiated austenitic stainless steels for different strain rate show that this material is not viscous [2]. Then, the material parameters A and m are adjusted in order to model time independent plasticity. Furthermore, because the dislocation channel is free irradiation defects, the hardening is limited and a weak hardening slope is chosen to model its plasticity behaviour. The slope is about $\mu/250$. The choice of this value is discussed in details in paragraph 5. The materials parameters have been also adjusted in order to have quasi-perfect plasticity behaviour (n, q, h_0, τ_{sat}) and have similar with the ones given by Anand et al. [25]. The influence of the initial critical shear stress τ_0 has been studied, and no significant influence has been observed if τ_0 is lower to the macroscopic tensile stress Σ_0. In the following, the initial critical shear stress is taken at 60 MPa [12]. Table 1 gives the material parameters used in this study.

Table 1
Material parameters used in the numerical simulations.

Parameters	A	m	n	q	h_0	τ_{sat}
Values	1×10^{-10}	0.01	1	1.4	250 MPa	65 MPa

3. Numerical results

3.1. Influence of the thickness and the length of the dislocation channel

In irradiated austenitic stainless steels, the thickness of dislocation channel can vary from 20 nm to 100 nm [2,31]. The thickness does not evolve with irradiation dose and depends probably on the type of austenitic stainless steels (304, 316), the experimental conditions and the initial heat-treatment (cold-worked or annealed). To study the influence of the thickness on the GB stress fields, three microstructures of the type M1 ($\alpha = 35°$), with t = 20 nm, 50 nm and 100 nm and for a length of L = 10 μm have been generated. Fig. 4 gives the GB normal and shear stress fields. A quasi-singularity of the GB stress fields is observed close to the intersection between the dislocation channel and GB. The GB shear stresses are about 70% smaller, at a distance of r = 5 nm of the dislocation channel, than the GB normal stresses. Consequently, it seems that the GB normal stresses control intergranular microcrack nucleation rather than GB shear stresses. Moreover, the numerical results show that if the thickness of the dislocation channel increases, the GB normal stresses increases. Near the dislocation channel (r = 5 nm), the normal stress reaches respectively for t = 20 nm, 50 nm and 100 nm: Σ_n = 750 MPa, 930 MPa and 1100 MPa for a tensile load of Σ_0 = 300 MPa. Consequently, more the dislocation channel is large more the material should be sensitive to intergranular crack nucleation.

The GB normal stresses are evaluated for two lengths of dislocation channel: L = 10 μm and L = 500 μm (in both cases t = 1 μm and the tensile load is equal to Σ_0 = 300 MPa). The computations are performed on the microstructure M1 ($\alpha = 35°$). The results (Fig. 5) show that the length of the dislocation channel influences strongly the GB normal stress. The larger the channel, the higher the GB normal stresses. Consequently, irradiated austenitic stainless steels with large grain size (the length of the dislocation channel is equal to about the grain size) will be probably more sensitive to intergranular microcrack nucleation. Lopez et al. [32] showed

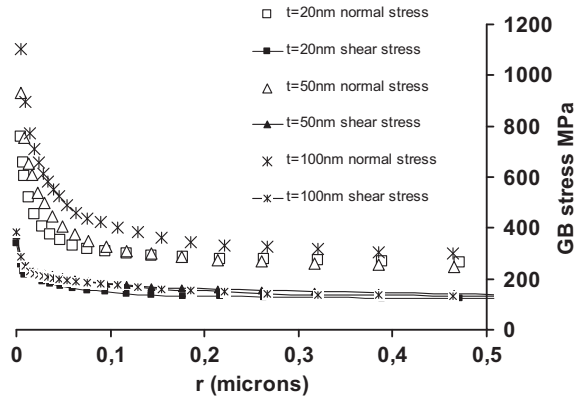

Fig. 4. GB normal and shear stresses for different thicknesses of the dislocation channel. Dislocation channelling and grain boundary intersection r = 0. (L = 10 μm, $\alpha = 35°$, Σ_0 = 300 MPa).

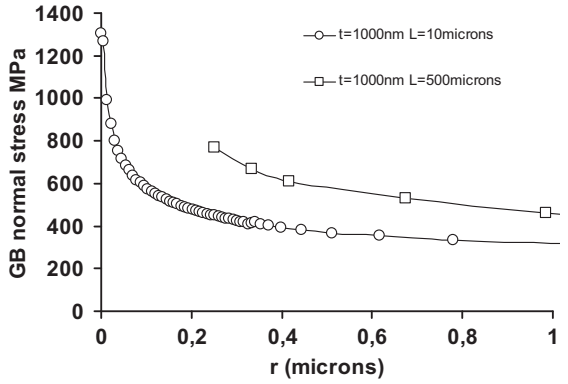

Fig. 5. GB normal stress for different lengths of the dislocation channel. Dislocation channelling and grain boundary intersection $r = 0$. ($\alpha = 35°$, $\Sigma_0 = 300$ MPa).

that austenitic stainless steels with large grain sizes are more sensitive to SCC than austenitic stainless steels with small grain sizes. Our numerical results are also in good agreement with experimental observations.

3.2. Influence of the grain boundary orientation with respect the tensile axis

The GB normal stress fields computed for the microstructures: M1 ($\alpha = 35°$) and M2 ($\alpha = 0°$) are plotted in Fig. 6. The thickness and the length of the dislocation channels are respectively $t = 50$ nm and $L = 10$ μm and the tensile load is equal to $\Sigma_0 = 300$ MPa. The remote GB normal stress can be computed by the following expression: $\Sigma_n^\infty = \Sigma_0 \cos^2\alpha$. For the microstructures M1 and M2, the remote GB normal stresses are respectively $\Sigma_n^\infty = 200$ MPa and $\Sigma_n^\infty = 300$ MPa. Near the dislocation channel (cf zoom Fig. 6), the GB normal stresses are quasi the same for both computations. On the contrary, far from the dislocation channel, the GB normal stress tends to the remote GB normal stress. Consequently, without dislocation channel the GB perpendicular to the macroscopic tensile axis are the most solicited. This result is coherent with the numerical results obtained by Kamaya et al. [33]. However, only two angles have been tested because testing many angles should be very time consuming. Following the Stroh [24] pile-up model (Fig. 7a), the GB normal stress field can be described as:

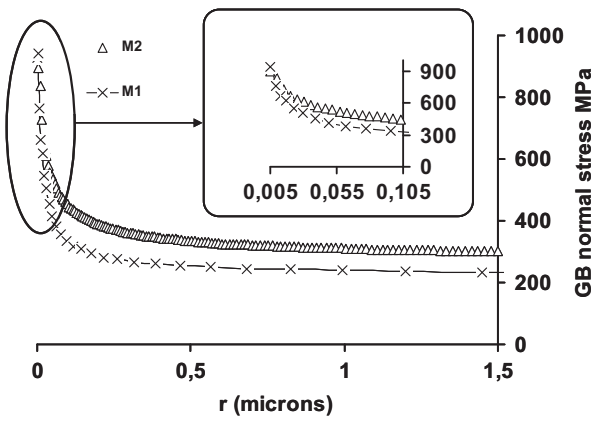

Fig. 6. GB normal stress for different orientations of the GB with respect the tensile axis (M1 $\alpha = 35°$, M2 $\alpha = 0°$). Dislocation channelling and grain boundary intersection $r = 0$. ($t = 50$ nm, $L = 10$ μm, $\Sigma_0 = 300$ MPa).

$$\Sigma_n = \frac{3}{2}\left(\frac{L^e}{r}\right)^{1/2}(\tau - \tau_0)h(\theta) \quad \text{with} \quad h(\theta) = \sin\theta\cos\frac{\theta}{2} \quad \theta \in [0;\pi] \tag{4}$$

where L^e and τ_0 are respectively the pile-up length and the initial critical shear stress. The resolved shear stress, τ, is computed by $\tau = f\Sigma_0$ where f is the Schmid factor ($f = 0.5$ for a well-oriented dislocation channel). The angle, θ, is defined between the pile-up and the GB (Fig. 7a), which can be expressed in function of α by $\theta = 45° + \alpha$ for a pile-up inclined to 45° with respect the tensile axis. Fig. 7b gives the evolution of the function: $g(\alpha) = h(45 + \alpha)$. For $\alpha = 0°$ and $\alpha = 35°$, Stroh model predicts a difference about 13% on the GB normal stress while FE computations predict a difference about 4% (at a distance of $r = 5$ nm of the dislocation channel). Thus, the analogy with the Stroh pile-up model can explain the small difference observed on FE computations. Furthermore, between $\alpha = -10°$ and $\alpha = 65°$, the function $g(\alpha)$ is quasi constant (±13%). The influence of GB orientation on GB normal stresses near the dislocation channel could be neglected in this angle range. On the contrary, the GB normal stresses, near the dislocation channel, should be depend of the GB orientation with respect the tensile axis for $\alpha < -10°$ and $\alpha > 65°$. However, for this angle range, from the Stroh pile-up model, the GB normal stress will be weak and no microcracks nucleation should be observed.

4. Analytical model and microcrack nucleation criterion proposition

4.1. Analytical model

Previous results have shown that the thickness and the length of the dislocation channel had a significant influence on the GB

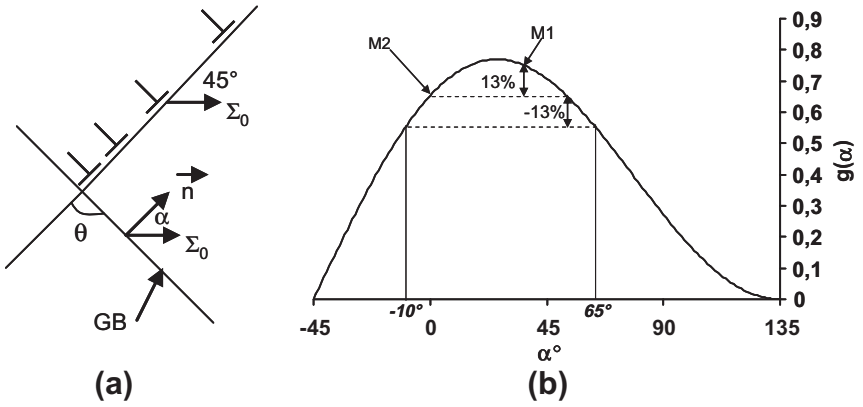

Fig. 7. (a) Pile-up model and (b) evolution of the function $g(\alpha)$ which described the dependence of the stress field with respect to the α angle.

normal stress fields. Furthermore, near the dislocation channel, the GB normal stresses are probably not influenced by the GB orientation with respect the tensile axis in a range of $\alpha \in [-10°; 65°]$. But far from the dislocation channel, the GB boundary normal stress tends to the remote GB normal stress. The Stroh pile-up model (Eq. (4)) has been compared to FE computations and the pile-up model overestimates strongly the GB normal stresses. Moreover, this one does not taken into account the influence of dislocation channel thickness which influences the GB normal stresses. In the purpose to formulate a microcraks nucleation criterion at the intersection channel-GB from the Griffith theory, we propose to predict the GB normal stresses by making an analogy with the elastic fracture mechanics theory and a singularity (as the Stroh pile-up model) in $1/\sqrt{r}$ is used to describe the GB normal stress field. Because, computations show that GB shear stresses are negligible, the following analytical model, in mode I, is also proposed to account for the GB normal stresses:

$$\Sigma_n = \frac{K_I}{\sqrt{2\pi r}} + \Sigma_n^{\infty} \tag{5}$$

Noted that this expression is validated if the GB orientation is such as $\alpha \in Z[-10°; 65°]$. The equivalent stress intensity factor (SIF), K_I, depends of the geometry of the crack (the dislocation channel in this study) and the load. The dislocation channel can be divided in two microcracks, one with a length 'L' and another with a length 't'. The following expression of the equivalent SIF is also proposed:

$$K_I = (f\Sigma_0 - \tau_0)(A\sqrt{t} + B\sqrt{L}) \tag{6}$$

A and B are two parameters which should be adjust on FE results. The both parameters are adjusted using three numerical results obtained using microstructure M1 (t = 1000 nm L = 500 μm, t = 1000 nm L = 10 μm, t = 50 nm L = 10 μm). Fig. 8 shows the comparison between stress fields either computed by FE model or by the analytical model using the adjusted parameters A = 3.14 and B = 0.14 (the fixed parameters are f = 0.5, Σ_0 = 300 MPa, τ_0 = 60 MPa and α = 35°). The analytical model is able to account for the influence of the thickness and the length of the dislocation channel on the GB normal stress fields. Moreover, the analytical model predicts correctly the values of GB normal stresses. The proposed analytical model is validated using other FE results obtained with various parameters: (i) thickness (t = 20 nm and t = 100 nm) (Fig. 9a), (ii) GB orientation (α = 0°) (Fig. 9b) and (iii) loads (Σ_0 = 500 MPa, Σ_0 = 700 MPa) (Fig. 9c).

(i) the proposed model is able to predict correctly the influence of the thickness. Near the dislocation channel at a distance of r = 5 nm (cf zoom Fig. 9a), the difference between the stress computed by the FE method and the analytical formula are 14% for t = 20 nm and 15% for t = 100 nm,

(ii) the proposed model predicts correctly the GB normal stress far from the dislocation channel. However, near the dislocation channel at a distance of r = 5 nm (cf zoom Fig. 9b), the

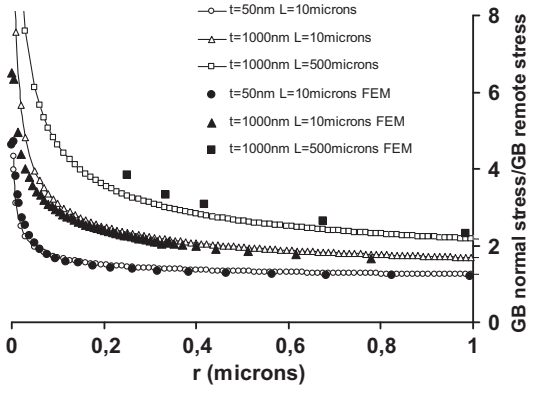

Fig. 8. Identification of the analytical model parameters. Comparison between stress fields computed either by the analytical model or the FE method for different thickness and length of dislocation channelling (α = 35°, Σ = 300 MPa).

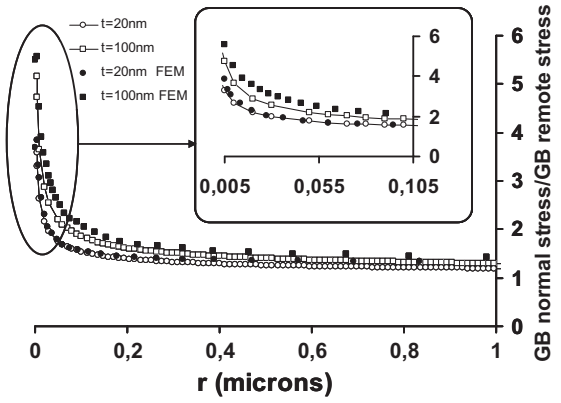

Fig. 9a. Validation of the analytical model. Comparison between stress fields computed either by the analytical model or the FE method for different thickness: t = 20 nm and t = 100 nm (L = 10 μm, α = 35°, Σ = 300 MPa).

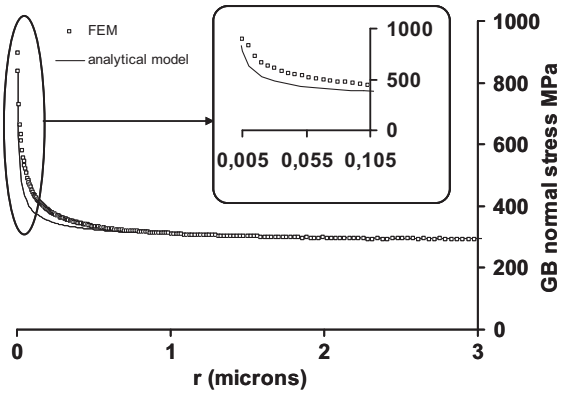

Fig. 9b. Validation of the analytical model. Comparison between stress fields computed either by the analytical model or the FE method for another orientation of the GB with respect to the tensile axis: α = 0° (t = 50 nm, L = 10 μm Σ = 300 MPa).

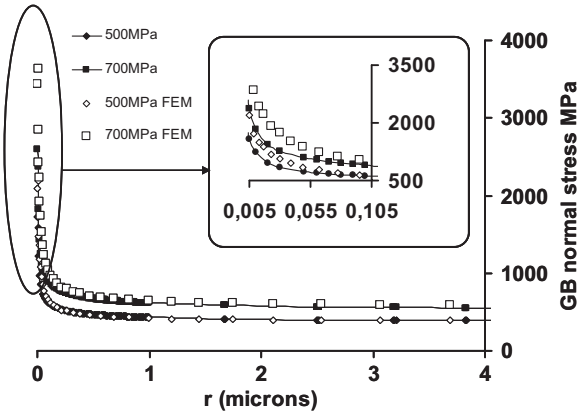

Fig. 9c. Validation of the analytical model. Comparison between stress fields computed either by the analytical model or the FE method for other loads: Σ_0 = 500 MPa, Σ_0 = 700 MPa (t = 50 nm, L = 10 μm, α = 35°).

analytical model underestimated the GB normal stress for a GB orientation of $\alpha = 0°$,

(iii) whatever the load, the analytical model predicts correctly the GB normal stress fields. However, the higher the load, the higher the difference between the analytical model and the FE results. Close to the dislocation channel (cf zoom Fig. 9c), at a distance of $r = 5$ nm, the difference between the stress computed by the FE method and the analytical formula are 27% for $\Sigma_0 = 500$ MPa and 34% for $\Sigma_0 = 700$ MPa.

4.2. Microcrack nucleation criterion proposition

As mentioned in introduction, during the initial phase of failure, intergranular microcracks nucleation is generally observed and the fractographies show a quasi brittle failure. These observations motivate to develop a microcracks nucleation criterion based on the elastic–brittle Griffith model. The crack area energy G can be computed from the SIF by:

$$G = \frac{K_I^2(1-\upsilon^2)}{E} \tag{7}$$

assuming plane strain, with E and ν, the Young modulus and the Poisson ratio respectively. The microcrack nucleates if G is equal to the fracture surface energy γ. In the case of intergranular cracking, the fracture surface energy is decomposed in two terms: $\gamma = 2\gamma_s - \gamma_{GB}$, where γ_s denotes free surface energy per unit area and γ_{GB} the GB energy per unit area. From Eqs. (6) and (7), an intergranular microcrack nucleation criterion is obtained. A microcrack nucleates if $\Sigma_0 > \Sigma_{crit}$ with Σ_{crit}:

$$\Sigma_{crit} = \frac{1}{f}\left(\sqrt{\frac{(2\gamma_s - \gamma_{GB})E}{1-\upsilon^2}}\frac{1}{A\sqrt{t} + B\sqrt{L}} + \tau_0\right) \tag{8}$$

The proposed criterion predicts that if the thickness or the length of the dislocation channel increases the stress to initiate microcrack decreases. Consequently, the austenitic stainless steels with large dislocation channel or grain sizes should be more sensitive to intergranular microcracks nucleation at the intersection channel-GB. In the next section, the influence of GB characteristics (non-CSL HABs, LABs, special GBs) and the environment on intergranular microcrack nucleation are discussed in the case of irradiated austenitic stainless steels.

5. Modelling of intergranular grain boundary microcrack nucleation

5.1. Grain boundary characteristic

Grain boundaries can be classified using the coincident site lattice (CSL) theory [34], which defines the periodicity, i.e., the degree of 'fit' between the two lattices. Using this model, it is possible to divide GB into categories [35,36], (i) low-angle boundary (LAB): up to 15° misorientation, (ii) non-CSL high-angle boundary (HAB) or general GBs and (iii) special GBs. The GB energy γ_{GB}, of LABs and special GBs is small, while the GB energy of non-CSL HABs is high [35,36]. The proposed criterion (Eq. (8)) predicts that the microcrack nucleation stress decreases when the GB energy increases. Consequently, non-CSL HABs should be more sensitive to intergranular microcrack nucleation than LAB and special GB. Dropek et al. [37] studied the influence of GB distribution on intergranular cracking for an irradiated austenitic stainless steel. The experimental results have shown that the material with a major part of non-CSL HABs are more sensitive to intergranular cracking that the material with a major part of LAB, and special GBs. The proposed criterion is also in good agreement with these experimental observations.

5.2. Intergranular microcrack nucleation in argon environment

Nishioka et al. [17] and Fukuya et al. [16] tested in argon environment austenitic stainless steels previously pre-irradiated to 35 dpa at a temperature of about 320 °C. The tensile tests have been carried out at very slow strain rate ($\approx 10^{-8}$ s^{-1}) and at a temperature of about 320 °C. In these experimental conditions, dislocation channels are observed at the surface of the specimens as well as close to the GBs. Both authors measured an experimental macroscopic microcrack nucleation stress close to the yield stress: i.e., $\Sigma_{crit}/\Sigma_y \approx 1$ (Fig. 10). Furthermore, Nishioka et al. observed no influence of the irradiation dose on the macroscopic microcrack nucleation stress from 4 dpa.

In the following, the predictions of the Smith and Barnby [38] and the proposed criterion (Eq. (8)) are compared to the previous experimental results. The microcrack nucleation stress predicted by the Smith and Barnby model is based on Stroh dislocation pile-up model [24]. The nucleation stress is computed assuming unfavourable conditions (i.e., $\theta = 70.5°$ and a well-oriented dislocation channel, Fig. 7a). The microcrack nucleation stress is computed by: $\Sigma_{crit}^{SB} = \sqrt{\frac{12\mu(2\gamma_s - \gamma_{GB})}{\pi(1-\upsilon)L^e}}$ where μ and L^e are respectively the elastic shear modulus and the length of the pile-up. Usually, the length of the pile-up is supposed to be the half of the grain size: $L^e = L/2$. The grain size and the dislocation channel thickness of austenitic stainless steels studied by Nishioka et al. [7] and Fukuya et al. [16] are about: $L = 50$ μm and $t = 50$ nm respectively. Uncertainties of ±20% are considered concerning the grain size and the dislocation channel thickness in the following computations. Without impurities located at GBs, the free surface energy for an austenitic stainless steel is in the range: $\gamma_s = 2$–3 J m^{-2} [39] and this one depends only slightly of the considered slip plane. The grain boundary energy, γ_{GB}, for an austenitic stainless steel, without impurities located at GBs, has been reported by Caul et al. [40] to be in an interval $\gamma_{GB} = 0.3$–1.2 J m^{-2}. On the contrary, these values depend strongly of the GB characteristic (LABs, special GBs, and non-CSL HABs). In order to apply both criteria to predict microcrack nucleation in argon environment, the free surface energy is

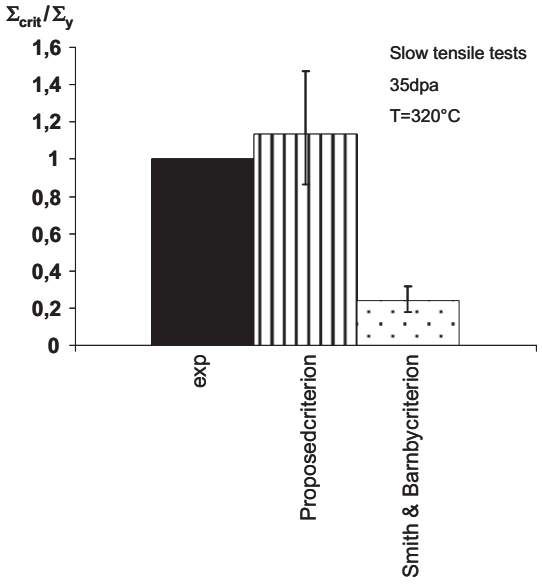

Fig. 10. Ratio Σ_{crit}/Σ_y (Σ_{crit}: macroscopic microcrack nucleation stress and Σ_y: macroscopic yield stress) for austenitic stainless steel pre-irradiated at 35 dpa ($T \approx 320$ °C) and tested in argon environment ($T \approx 320$ °C). Comparison between experimental results [7,16], and the predictions given by proposed criterion as well as the Smith and Barnby criterion (pile-up model). $t = 50$ nm (±20%), $L = 50$ μm (±20%), $f = 0.5$, $\tau_0 = 60$ MPa.

chosen to be 2.5 J m^{-2} and the minimum and maximum free surface energies of 2 J m^{-2} and 3 J m^{-2} are respectively considered, according to [39]. Concerning, the GB energy value, non-CSL HABs are the most sensitive to microcrack nucleation [37], we consider the highest GB energy which is γ_{GB} = 1.2 J m^{-2} according to [40]. The yield stress is considered to be equal to Σ_y = 1000 MPa (±20%) [5]. The results reported in Fig. 10 shows that the Smith and Barnby criterion, based on the Stroh pile-up model, underestimates strongly the microcrack nucleation stress. This result confirms that pile-up models are not well suited to predict the intergranular microcrack nucleation stress in pre-irradiated austenitic stainless steels. On the contrary, the proposed criterion (Fig. 10) is able to correctly predict the microcrack nucleation stress (see the scatter bar). It should be noticed that no adjustable parameter was used to apply the proposed criterion (Eq. (8)). However, in order to completely validate the proposed criterion, this one should be tested on other material (copper or nickel for example), which have another grain size and dislocation channel thickness. This future work represents also a perspective of the present work.

5.3. Intergranular microcrack nucleation in PWR environment

Recently [17,18] carried out uniaxial constant load (UCL) tests in PWR environment on pre-irradiated austenitic stainless steels (38 dpa). They measured the maximum stress for which failure occurred (named IASCC failure stress). In the experimental conditions of their tests (temperature about 300 °C and constant load) it is reasonable to assume that dislocation channel formed and contributed to intergranular microcrack nucleation and failure. The experimental results (Figs. 14 and 15) show that at 38 dpa, the ratio Σ_{crit}/Σ_y is equal to about 0.5, while this ratio at the same irradiation dose is equal to about 1 in argon environment as mentioned previously. In the next sections, we discuss independently the role of hydrogen embrittlement and oxidation, on the lower value of the ratio Σ_{crit}/Σ_y for pre-irradiated material tested in PWR environment.

5.3.1. Effect of hydrogen

Fujimoto et al. [41] measured the hydrogen concentration versus the irradiation dose in a 316CW (cold-worked) austenitic stainless steel irradiated in PWR environment. The authors observed that the hydrogen concentration increases from 400 appm at 0 dpa to 3000 appm at 35 dpa. However, in the same experimental conditions [42] measured a hydrogen concentration about 400 appm at 0 dpa, but this one does not increase with the irradiation dose. And, according to [41] the difference between both results seems difficult to explain.

The presence of hydrogen atoms at GBs could affect the fracture surface energy (γ). Rice and Wang [43] proposed an analytical model to take into account the presence of impurities (hydrogen in our case) at the GBs on the fracture surface energy. This model assumes that the thermodynamic system is in local equilibrium, symmetrical GB. The relation established by the authors is expressed by:

$$(2\gamma_S - \gamma_{GB})^1 = (2\gamma_S - \gamma_{GB})^0 - (\Delta g^0_{GB} - \Delta g^0_S)\Gamma \quad (9)$$

where $(2\gamma_s - \gamma_{GB})^0$ and $(2\gamma_s - \gamma_{GB})^1$, are respectively, the fracture surface energy without and with hydrogen atoms, Δg^0_{GB} and Δg^0_s , the Gibbs energy of the impurities at the grain boundary and at the free surface and Γ, the number of hydrogen atoms per square meter located at the GBs which is assume to be divided equally between tow surfaces. The equilibrium occupancy fraction of hydrogen is defined by: $\theta = \Gamma/\Gamma_s$, where Γ_s is the maximum number of hydrogen atoms at the GBs. In the case of FCC metals or alloys, this one is equal to about $\Gamma_s = 1.28 \times 10^{-19}$ atoms/m^2 = 2.13×10^{-5} mol/m^2. Recent ab initio computations performed by Geng et al. [44], Young et al. [45] and Yamaguchi et al. [46] on a nickel Σ5 twist or tilt GB (special GB) allowed them to compute the Gibbs energies. The authors found Gibbs energy (i.e., $\Delta g^0_{GB} - \Delta g^0_S$) comprises between 25 kJ/mol and 40 kJ/mol. The ratio $\frac{\gamma^1}{\gamma^0} = \frac{(2\gamma_S - \gamma_{GB})^1}{(2\gamma_S - \gamma_{GB})^0}$ for both values of Gibbs energy in a nickel Σ5 twist or tilt grain boundary is also plotted versus the equilibrium occupancy fraction of hydrogen θ (Fig. 11). Furthermore, from ab initio computations [47,48] have computed the free surface energy on a (1 1 1) surface versus occupancy fraction of hydrogen θ for aluminium. Their results are also plotted in Fig. 11. We can observe that the fracture surface energy is only slightly modified for a nickel Σ5 twist or tilt grain boundary (decrease of 20%), while in the case of aluminium, the free surface energy is strongly modified (decrease of 60%). The equilibrium occupancy fraction of hydrogen θ, can be computed by Hondros et al. [49] and Hirth [50]:

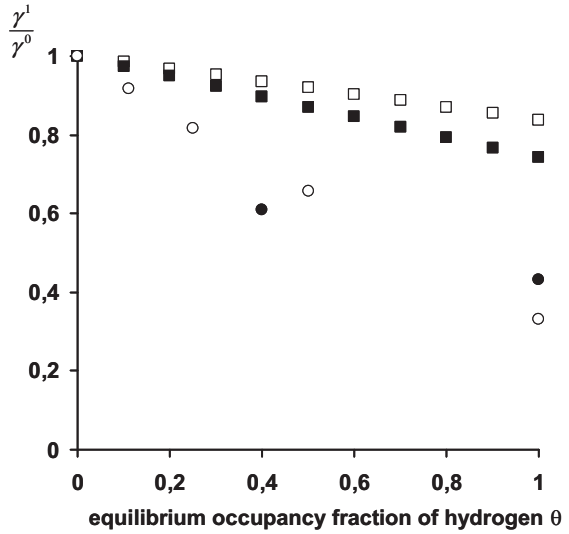

Fig. 11. Decrease of the normalized fracture surface energies versus equilibrium occupancy fraction of hydrogen: □ nickel Σ5 grain boundary $\Delta g^0_{GB} - \Delta g^0_S$ = 25 kJ/mol, $\gamma^0 = (2\gamma_s - \gamma_{GB})^0$ = 3.3 J/m^2 [44] ■ nickel Σ5 grain boundary $\Delta g^0_{GB} - \Delta g^0_S$ = 40 kJ/mol, $\gamma^0 = (2\gamma_s - \gamma_{GB})^0$ = 3.3 J/m^2 [45], ○ fcc aluminium along (1 1 1) free surface [48] $\gamma^0 = 2\gamma_s 0$ = 2.3 J/m^2 ● fcc aluminium along (1 1 1) free surface [47] $\gamma^0 = 2\gamma_s 0$ = 2 J/m^2.

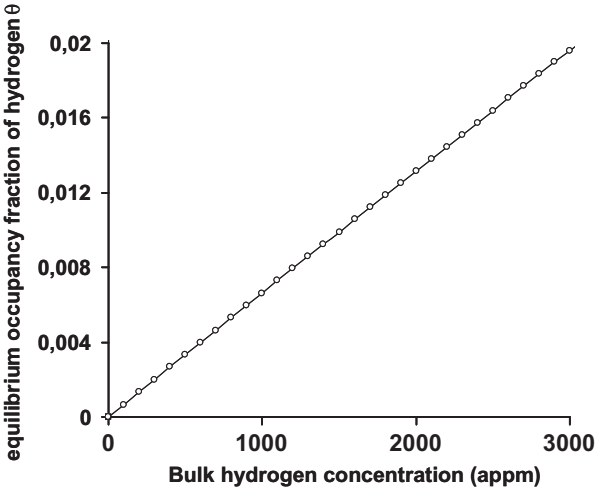

Fig. 12. Grain boundary equilibrium occupancy fraction of hydrogen versus the bulk hydrogen concentration Eq. (10) (ΔH_b = 20 kJ/mol, T = 573 K, R = 8.31 J mol^{-1} K^{-1}).

$$\frac{\theta}{1-\theta} = C_0 \exp\frac{\Delta H_b}{RT} \tag{10}$$

where C_0 is the hydrogen concentration (appm), ΔH_b the GB binding energy (kJ/mol), T the temperature (K). This expression is plotted versus hydrogen concentration (Fig. 12) considering PWR water temperature (573 K) and $\Delta H_b = 20$ kJ/mol [51]. It can be observed that for a hydrogen concentration comprises between 500 and 3000 appm, the equilibrium occupancy fraction of hydrogen is comprised between 0.003 and 0.02. Consequently, this model coupled with the Rice and Wang model [43] lead to a fracture surface energy which is not modified by the hydrogen atoms at the GBs. This cannot explain the lowest value of the IASCC macroscopic nucleation stress at high dose for material tested in PWR environment in comparison to material tested in argon environment.

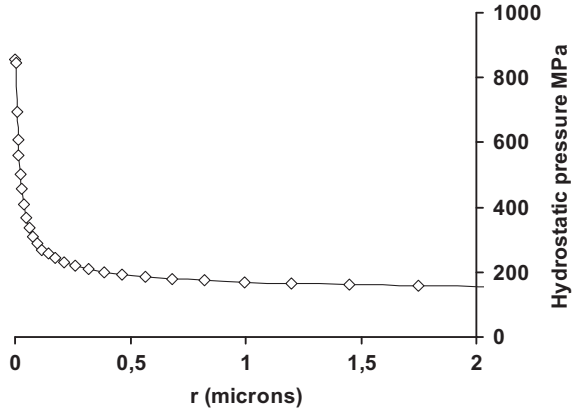

Fig. 13. Grain boundary hydrostatic pressure obtained from finite element computation. Dislocation channelling and grain boundary intersection $r = 0$ ($t = 50$ nm, $L = 10$ μm, $\tau_0 = 60$ MPa, $\alpha = 35°$, $\Sigma_0 = 300$ MPa).

However, hydrogen atoms can be trapped if the hydrostatic pressure $p = Tr(\sigma)/3$, is sufficiently high. The hydrostatic pressure at the GB has been computed using the FE method (Fig. 13). A quasi-singularity of the GB hydrostatic stress is observed close to the intersection between the dislocation channel and the GB. The hydrostatic pressure reaches about 900 MPa close to the dislocation channel for a tensile load of $\Sigma_0 = 300$ MPa. Consequently, it is probable that hydrogen diffuse toward the intersection between dislocation channel and the GB. Let us assume that $\theta = 1$ at the GB close to the dislocation channel. If austenitic GBs have the same behaviour as the nickel GBs, with respect to hydrogen embrittlement, the fracture surface energy would decrease of 20% (i.e., from $2\gamma_s - \gamma_{GB} = 3.8$ J m^{-2} to $2\gamma_s - \gamma_{GB} = 3$ J m^{-2}). On the contrary, if austenitic free surface follow the same behaviour as the aluminium free surface, with respect the hydrogen embrittlement, the free surface energy decreases of 60% (i.e., from $2\gamma_s = 5$ J m^{-2} to $2\gamma_s = 2$ J m^{-2}). Unfortunately, we are not aware of any study allowing the computation or measurement of the energies of aluminium GBs containing hydrogen. Then, we assume that the GB energy is not strongly affected by hydrogen atoms and a value of $\gamma_{GB} = 1.2$ J m^{-2}, according to [40] is also used (i.e., $2\gamma_s - \gamma_{GB} = 0.8$ J m^{-2}). These values are used to compute macroscopic nucleation stress predicted by either the proposed criterion or the Smith and Barnby criterion at a dose of 38 dpa. In these computations, the grain size, the dislocation channel thickness and the yield stress are considered to be equal to $L = 50$ μm (±20%), $t = 50$ nm (±20%) and $\Sigma_y = 1000$ MPa (±20%), respectively. The results (Fig. 14a and b) show that the Smith and Barnby criterion underestimates the IASCC nucleation stress whatever the hydrogen embrittlement sensitivity (Ni or Al behaviour predicted by the ab initio computations). The proposed criterion overestimates the IASCC nucleation stress if

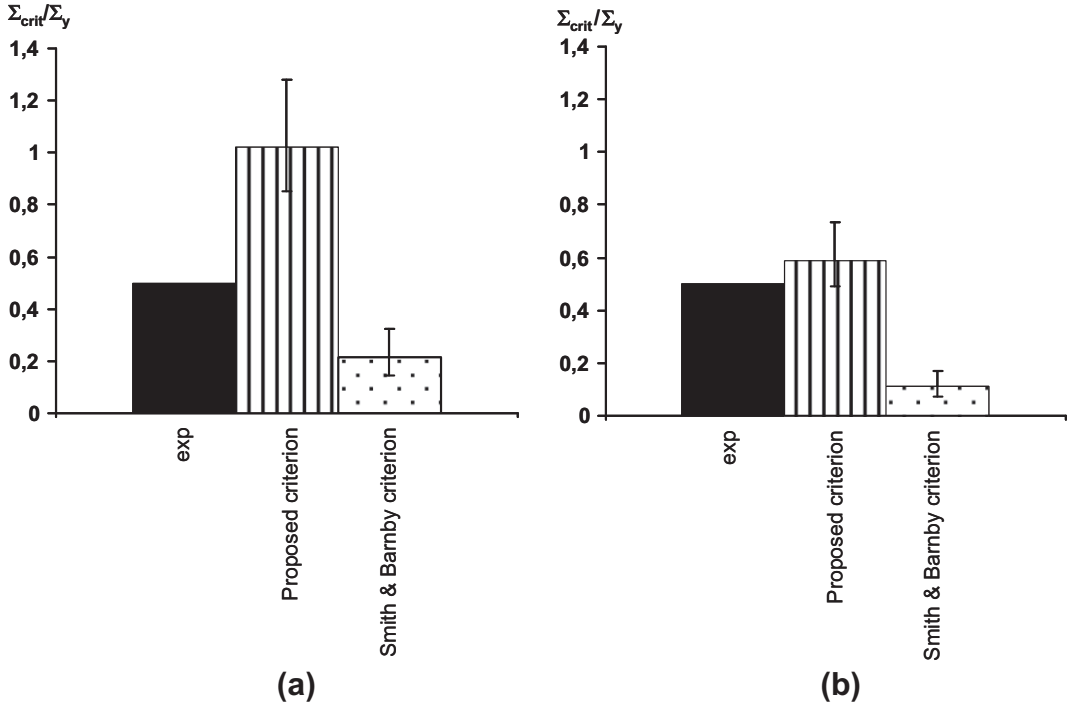

Fig. 14. Ratio Σ_{crit}/Σ_y (Σ_{crit}: macroscopic microcrack nucleation stress and Σ_y: macroscopic yield stress) for an irradiated austenitic stainless steel pre-irradiated at 35 dpa ($T \approx 320$ °C) and tested in PWR environment ($T \approx 320$ °C). Comparison between experimental results [17,18], and predictions given by the proposed criterion as well as the Smith and Barnby criterion ($t = 50$ nm (±20%), $L = 50$ μm (±20%), $f = 0.5$, $\tau_0 = 60$ MPa). Predictions taking into account hydrogen embrittlement with a GB occupancy of $\theta = 1$ (Fig. 12), (a) using the fracture surface energy computed for nickel $\Sigma 5$ grain boundary $2\gamma_s - \gamma_{GB} = 3$ J m^{-2} (Fig. 11), (b) using the fracture surface energy computed for aluminium $2\gamma_s - \gamma_{GB} = 0.8$ J m^{-2} (Fig. 11).

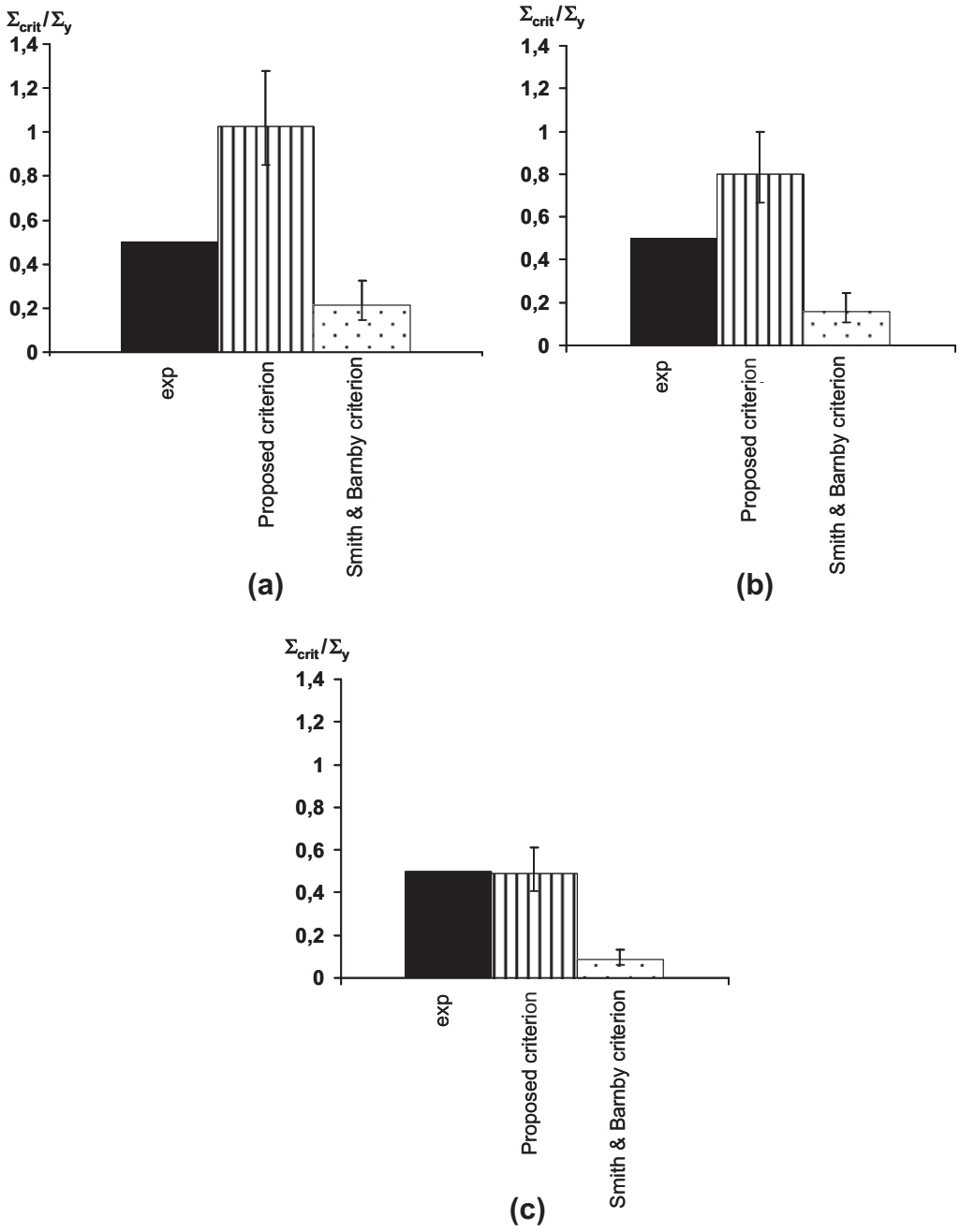

Fig. 15. Ratio Σ_{crit}/Σ_y (Σ_{crit}: macroscopic microcrack nucleation stress and Σ_y: macroscopic yield stress) for an irradiated austenitic stainless steel pre-irradiated at 35 dpa ($T \approx 320$ °C) and tested in PWR environment ($T \approx 320$ °C). Comparison between experimental results [17,18], and predictions given by the proposed criterion as well as the Smith and Barnby criterion ($t = 50$ nm (±20%), $L = 50$ μm (±20%), $f = 0.5$, $\tau_0 = 60$ MPa), (a) using the fracture surface energy computed for pure Fe_2O_3, $2\gamma_s - \gamma_{GB} = 3$ J m^{-2}, (b) using the fracture surface energy computed for hydrated Fe_2O_3, $2\gamma_s - \gamma_{GB} = 1.7$ J m^{-2}, (c) using the fracture surface energy computed for hydroxylated Fe_2O_3, $2\gamma_s - \gamma_{GB} = 0.5$ J m^{-2}.

we consider that the austenitic GBs follow the same behaviour that nickel GBs (Fig. 14a). On the contrary, if we consider that the austenitic GBs follow the same behaviour that aluminium GBs (Fig. 14b), the proposed criterion is able to correctly predict the IASCC macroscopic nucleation stress. In a future work, ab initio computations should be performed on Fe–Ni–Cr with the presence of hydrogen atoms at GB in order to have a more precise values of fracture surface energy.

5.3.2. Effect of oxidation

Asano et al. [52], Bruemmer et al. [1] and Miwa et al. [53] measured the GB chromium concentration in pre-irradiated austenitic stainless steels. They observed that the chromium concentration decreases when the irradiation dose increases. The minimum concentration reaches about 11% at 10 dpa. Furthermore, an enrichment of nickel is observed at the GBs. The GB chemical composition variations are due to the Kirkendall inverse effect (see for example [1,11]), Then, it is probable that at the intersection between the free surface and the GB, the oxide layer can be break by the combined effect of dislocation channel and the depletion of chromium which does not allow the repassivation of the oxide layer. Oxygen can also diffuse inside the material. Oxide such as Fe_2O_3, Fe_3O_4, Cr_2O_3, NiO can be formed and embrittle GBs [54]. The fracture surface energy is also modified by the presence of

oxide. At 38 dpa, GB chromium content is too low for continuous repassivation and the GBs can be oxidized. Free surface energies per unit area have been calculated for Fe_2O_3, Fe_3O_4, Cr_2O_3, or NiO oxides using ab initio computations. The obtained values are about $2\gamma_s = 3$–$5\ J\ m^{-2}$ [55,56]. Leeuw et al. [57] computed free surface energy $2\gamma_s$, for pure, hydrated and hydroxylated Fe_2O_3. They obtained respectively, $2\gamma_s = 4.2\ J\ m^{-2}$, $2\gamma_s = 2.9\ J\ m^{-2}$ and $2\gamma_s = 1.7\ J\ m^{-2}$. Unfortunately, we are not aware of any study allowing the computation or measurement of GB energies for these oxides. Consequently, a GB energy of $\gamma_{GB} = 1.2\ J\ m^{-2}$ is used [40] which gives the right order of magnitude for non-CSL HABs for various materials [35]. From [57] results, three applications of the proposed and Smith and Barnby criteria are performed using: (i) fracture surface energy of $2\gamma_s = 4.2\ J\ m^{-2}$ minus a GB energy of $\gamma_{GB} = 1.2\ J\ m^{-2}$ (i.e., $2\gamma_s - \gamma_{GB} = 3\ J\ m^{-2}$), (ii) fracture surface energy of $2\gamma_s = 2.9\ J\ m^{-2}$ minus a GB energy of $\gamma_{GB} = 1.2\ J\ m^{-2}$ (i.e., $2\gamma_s - \gamma_{GB} = 1.7\ J\ m^{-2}$) and (iii) fracture surface energy of $2\gamma_s = 1.7\ J\ m^{-2}$ minus a GB energy of $\gamma_{GB} = 1.2\ J\ m^{-2}$ (i.e., $2\gamma_s - \gamma_{GB} = 0.5\ J\ m^{-2}$). As before, the grain size, the dislocation channel thickness and the yield stress are chosen to be: $L = 50\ \mu m$ (±20%), $t = 50$ nm (±20%) and $\Sigma_y = 1000$ MPa (±20%) respectively. The results (Fig. 15a–c) show that the Smith and Barnby criterion underestimates the IASCC stress whatever the fracture surface energy. Using the fracture surface energy of $2\gamma_s - \gamma_{GB} = 3\ J\ m^{-2}$, pure Fe_2O_3 and $2\gamma_s - \gamma_{GB} = 1.7\ J\ m^{-2}$, hydrated Fe_2O_3 (Fig. 15a and b), the proposed criterion underestimates the IASCC stress. However, with a fracture surface energy of $2\gamma_s - \gamma_{GB} = 0.5\ J\ m^{-2}$, hydroxylated Fe_2O_3 (Fig. 15c), the proposed criterion is able to correctly predict the IASCC stress.

5.3.3. Summary

It is probable that hydrogen embrittlement and oxidation participle together to IASCC nucleation. Other studies should be performed to know how to take into account both effects in the modelling. Finally, another effect should be participle to material embrittlement such as helium bubbles formation at GB [58]. This last embrittlement mechanism should be study in a future work.

6. Discussion

6.1. Continuum versus discrete approaches

Continuum approach does not allow us to predict the spatial distribution of the dislocations in the channel. Therefore, the GB stress field induced by the real distribution of dislocations in the channel cannot be computed accurately. This spatial distribution depends on the dislocation sources, cross-slip events (eventually climb), inter-dislocation stresses. Using the stress field induced by each dislocation, it would be finally possible to compute a more physically-based GB stress field than the one computed using continuum modelling. Such computations would require us to carry out discrete dislocation dynamics (DDD) computations which are much more time consuming than crystalline FE computations. Furthermore, the exact mechanisms of channel production are still in debate and depend very probably on the irradiation defect characteristics (SFT, Frank loop) and temperature. Following the results of DDD reported in the literature several mechanisms should be involved such as cross-slip [59,60,15], climb [60] and pile-ups [59,15]. On the experimental point of view, the in situ TEM observations of Robach et al. carried out on polycrystalline copper [61] show that screw dislocations are indeed more efficient than edge dislocations for annihilating irradiation defect. They show that channelling results in addition from the effect of numerous dislocations located in pile-ups. All these mechanisms may affect the spatial distribution of dislocations in the channels and therefore the induced GB stress fields.

It should nevertheless be noticed that our basic continuum approach permits us to investigate the influence of many parameters such as channel thickness and length, elasticity and plasticity parameters, grain boundary orientation, and applied stress. An analytical formula is even be deduced allowing the evaluation of the GB stress fields for various materials and configurations.

Chou and Li studied the stress field induced by parallel pile-ups which may carry out the slip instead of a single pile-up [62]. A stress singularity is found close to each small pile-up (l: length of each small pile-up, $l < L$), particularly on each side of the channel. It is due to the assumption of elastic behaviour outside the channel. The stress singularity would be of $\sqrt{l/r}$ type if the distance between the small pile-up is large enough (see below the range of validity of the pile-up stress fields).

The square root singularity found using the discrete or continuum approaches is based on the assumption of elastic behaviour outside the channel. This hypothesis is based on some experimental observations. The etch-pit observations of Young showed that only a low fraction of the dislocation segments located outside channels glide during tensile deformation [63]. For a neutron irradiation dose higher than 10 dpa at a temperature of 320 °C, the dislocation segment density measured after irradiation is very low ($<10^{11}\ m^{-2}$ following [30]). Therefore, the probability of finding a dislocation segment in the stress concentration area around the intersections of channels and GBs is very low. This means that slip activation from pre-existing dislocation segments is very rare, except in channels. And the stress required for nucleating mobile dislocation segments from GBs are very high following recent molecular dynamics computations investigating various metals and GB kinds [64]. This is why the assumption of elastic behaviour outside the channels seems reasonable. One exception would be the case of special boundaries such as twin boundaries for which slip transfer in the next grain has been observed [65]. This should lead to stress relaxation.

Some limitations concerning the validity of the stress field singularity should be mentioned. First, the elastic stress field induced by a dislocation is only valid at a distance larger than the core radius, r_{core}, which is about three times the Burgers vector length, b ($r_{core} \geqslant 1$ nm). Second, the pile-up stress singularity has another limitation detailed by Stroh [4]. This is not valid close to the head of the pile-up. For edge dislocation pile-ups, the cut-off length is given by Stroh [4]:

$$r \gg r_{cut\text{-}off} = \frac{\mu}{4\pi(1-\nu)T} b$$

with μ the elastic shear modulus, υ the Poisson ratio and T the applied shear stress. For the tests studied in our article (austenitic stainless steels, neutron doses higher than a few dpa, temperature of about 300 °C), $T \approx 250$–500 MPa (one half of the axial stress), this leads to: $r_{cut\text{-}off} \approx 15$–$30b > r_{core}$. As mentioned by Stroh, in the range $[r_{core}, r_{cut\text{-}off}]$, the stress singularity due the dislocation at the head of the pile-up dominates, which leads to a singularity of type: $\mu b/r$. For a distance to the pile-up dislocation lower than the core radius, the elastic fields are of course no more valuable. Therefore, because of the cruder assumptions of the continuum approach presented here, the stress fields computed by the FE method are not valid if the distance to the channel-GB intersection is lower than $r_{cut\text{-}off} \approx 15$–$30b$.

6.2. Channel hardening

Sharp observed by TEM the channel microstructure formed during tensile deformation at room temperature of pre-irradiated copper well-oriented single crystals [66]. Sharp concluded that the microstructure is composed mainly of primary dislocations and edge dipole bundles. This microstructure seems very similar to the one formed during the first stage of tensile deformation of

non-irradiated copper crystals oriented for single slip. Following [67–70], the stage I deformation in FCC well-oriented single crystals is characterized by a plastic tangent modulus belonging to the range $\mu/200$–$\mu/2000$, depending on the plastic slip range and material (aluminium, copper). This modulus is defined by the ratio between the resolved shear stress and plastic slip increments. As explained in paragraph 1, a very weak hardening slope was used, about $\mu/250$. It was uneasy to use a weaker value because of numerical convergence problems.

The polycrystal hardening is much higher than the single crystal hardening, either for the unirradiated or pre-irradiated austenitic stainless steel [5]. This hardening is due to pile-ups and grain to grain interactions which are negligible in single crystals. For example the high channel deformation induces high long-range stresses are automatically computed by the FE method. They lead to high polycrystalline hardening.

Finally, still following TEM observations [66], Sharp noticed that the strain rate does not affect the channel dislocation microstructure, which agrees with the results of macroscopic tensile tests. Neglecting viscosity in the studied loading conditions seems therefore physically based.

6.3. Effect of neighbour grains

Neighbour grains may affect the local stress level in a given grain. As austenitic stainless steels present a high anisotropy level of crystalline elasticity ($a = 2C_{44}/(C_{11} - C_{12}) = 3.3$), this effect is particularly visible at low stress for which crystalline elasticity is dominant. Crystalline FE computations show that the scatter on the resolved shear stress induced by the random orientations of neighbour grains of similar equiaxed geometry is about ±16% [71,72]. In addition, computations taking into account slip bands in the considered grain, show that the channel plastic slip scatter is even higher: ±30% [73]. This is due to the channel non-linear behaviour. Nevertheless, elastic strain measurements [74] and computations carried out for higher plastic strains [74,75], corresponding to generalized plasticity in the polycrystal show that the scatter of the mean grain plastic strain distribution decreases dramatically with the macroscopic strain increasing. And the computations taking into account the variable orientation of the next grain lead to negligible scatter of the GB stress field close to the channel-GB intersection. Further computations taking into account a larger number of grains and higher plastic strains are required for evaluating the scatter in the GB stress fields induced by the random orientations of the neighbour grains.

7. Conclusions

In order to study the role played by dislocation channel on intergranular microcrack nucleation in pre-irradiated austenitic stainless steel, finite element computations are performed using crystal plasticity law and meshes including a channel of finite thickness. The influence of dislocation channel on grain boundary stress field has been studied. The numerical results show that the dislocation channel thickness and length influence strongly the grain boundary normal stresses. An analytical model, with a stress singularity as $1/\sqrt{r}$ (r: distance to the dislocation channel-grain boundary intersection) is proposed, for which a stress intensity factor, applied to dislocation channel impacting a grain boundary, is formulated. The analytical model is adjusted using few finite element results and is validated with other finite elements results. From the analytical model, a grain boundary microcrack nucleation criterion is deduced, based on the elastic–brittle Griffith model. The proposed criterion predicts correctly the influence of grain boundary characteristics (LABs, non-CSL HABs, special GBs) on intergranular cracking observed in pre-irradiated austenitic stainless steels. Furthermore, the proposed criterion predicts correctly the macroscopic grain boundary microcrack nucleation stress for pre-irradiated austenitic stainless steels tested at low strain rate in argon environment. On the contrary, the Smith and Barnby criterion, based on the Stroh dislocation pile-up model underestimates strongly the microcrack nucleation stress. This shows that the pile-up model is not well suited to predict the grain boundary microcrack nucleation of deformed pre-irradiated austenitic stainless steels. To predict microcrack nucleation stress in PWR environment, ab initio computation results from the literature are used to obtain the fracture surface energies modified by the presence of hydrogen atoms or oxide at grain boundaries. The results show that the Smith and Barnby criterion still underestimates strongly the IASCC macroscopic nucleation stress. On the contrary, some of the fracture surface energies deduced from ab initio computations of the literature allows to correctly predicting the IASCC macroscopic nucleation stress with the proposed criterion.

Acknowledgments

This work was partially supported by the project PERFORM60 of the Euratom framework programme 7th FWP, under contract No.: 232612 and the CEA research program DEN/DSNI/RSTB/RACOC. We are grateful to Dr. Bernard Marini and Dr. Benoît Tanguy for interesting discussions.

References

[1] S.M. Bruemmer, E.P. Simonen, P.M. Scott, P.L. Andresen, G. S Was, J.L. Nelson, J. Nucl. Mater. 274 (1999) 299.
[2] N. Hashimoto, S.J. Zinkle, A.F. Rowcliffe, J.P. Robertson, S. Jitsukawa, J. Nucl. Mater. 283–287 (2000) 528.
[3] K. Farrell, T.S. Byun, N. Hashimoto, J. Nucl. Mater. 335 (2004) 471.
[4] T.S. Byun, K. Farrell, J. Nucl. Mater. 326 (2004) 86.
[5] C. Pokor, Y. Brechet, P. Dubuisson, J.P. Massoud, X. Averty, J. Nucl. Mater. 326 (2004) 30.
[6] N. Hashimoto, T.S. Byun, K. Farrell, J. Nucl. Mater. 351 (2006) 295.
[7] H. Nishioka, K. Fukuya, K. Fujii, Y. Kitsunai, J. Nucl. Sci. Technol. 45 (2008) 274.
[8] T. Tsukura, Y. Miwa, H. Tsuji, H. Nakajima, J. Nucl. Mater. 258–263 (1998) 1669.
[9] J.I. Cole, H. Tsai, T.R. Allen, T. Yoshitake, N. Akasaka, I. Yamagata, Y. Nakamura, J. Nucl. Mater. 351 (2006) 316.
[10] T.S. Byun, K. Farrell, E.H. Lee, L.K. Mansur, S.A. Maloy, M.R. James, W.R. Johnson, J. Nucl. Mater. 303 (2002) 34.
[11] G. Was, Springer, Netherlands, 235, 2007 (Chapter 15).
[12] M. Sauzay, K. Bavard, W. Karlsen, J. Nucl. Mater., in press.
[13] A. Toivonen, U. Ehrnstén, W. Karlsen, P. Aaltonen, J.-P. Massoud, J.-M. Boursier, in: Proceedings of the 12th International Conference on Environmental Degradation of Materials in Nuclear Power System, 2005.
[14] Y. Osetsky, D. Rodney, D. Bacon, Phil. Mag. 86 (2006) 2295.
[15] T. Nogaret, D. Rodney, M. Fivel, C. Robertson, J. Nucl. Mater. 380 (2008) 22.
[16] K. Fukuya, H. Nishioka, K. Fujii, T. Torimaru, J. Nucl. Sci. Technol. 45 (2008) 452.
[17] H. Nishioka, K. Fukuya, K. Fujii, T. Torimaru, J. Nucl. Sci. Technol. 45 (2008) 1072.
[18] K. Takakura, K. Nakata, K. Sakima, K. Fujimoto, N. Kubo, Workshop, Beaune, France, 2007.
[19] Z. Jiao, G.S. Was, J. Nucl. Mater. 382 (2008) 203.
[20] L. Fournier, M. Savoie, D. Delafosse, J. Nucl. Mater. 366 (2007) 187.
[21] T.S. Byun, N. Hashimoto, J. Nucl. Mater. 354 (2006) 123.
[22] Z. Jiao, J.T. Busby, R. Obata, G.S. Was, in: Proceedings of the 12th International Conference on Environmental Degradation of Materials in Nuclear Power Systems – Water Reactors, The Minerals, Metals and Materials Society, 2005, pp. 379.
[23] http://www-cast3m.cea.fr.
[24] A.N. Stroh, Proc. Roy. Soc. A223 (1954) 404.
[25] L. Anand, S. Balasubramanian, K. Kothari, in: Ch. Teodosiu (Ed.), CISM Courses and Lectures No. 376, 1996.
[26] S. Héraud, PhD Thesis, Ecole Polytechnique, Palaiseau, France, 1998.
[27] E. Ferrie, M. Sauzay, J. Nucl. Mater. 386–388 (2009) 666.
[28] F.A. McClintock, A.S. Argon, Mechanical Behaviour of Materials, Addison-Wesley Publishing Company, 1966.
[29] H.B. Huntington, in: F. Seitz, D. Turnbull (Eds.), Solid State Physics, vol. 7, Academic Press Corporation Publishers, New-York, 1958, pp. 214–243.
[30] C. Pokor, Y. Brechet, P. Dubuisson, J.P. Massoud, X. Averty, J. Nucl. Mater. 326 (2004) 19.
[31] E. H Lee, T.S. Byun, J.D. Hunn, K. Farrel, L.K. Mansur, J. Nucl. Mater. 26 (2001) 183.

[32] H.F. Lopez, M.M. Cisneros, H. Mancha, O. Garcia, M.J. Pérez, Corros. Sci. 48 (2006) 913.
[33] M. Kamaya, Y. Kawamura, T. Kitamura, Int. J. Solids Struct. 44 (2007) 3267.
[34] M.L. Kronberg, F.H. Wilson, Trans. Metal. Soc. AIME 185 (1949) 501.
[35] A.P. Sutton, R.W. Balluffi, Clarendon Press, Oxford, 1995.
[36] L. Priester, De la théorie à l'ingénierie, EDP Sciences, 2006.
[37] R.B. Dropek, G.S. Was, J. Gan, I. Cole, T.R. Allen, E.A. Kenik, in: 11th Int. Conf., American Nuclear Society, La Grange Park, IL, 2004, pp. 1132.
[38] E. Smith, J.T. Barnby, Metal Sci. J. 1 (1967) 56.
[39] L. Vitos, A.V. Ruban, H.L. Skriver, J. Kollar, Surf. Sci. 411 (1998) 186.
[40] M. Caul, J. Fiedler, V. Randle, Scripta Mater. 35 (1996) 831.
[41] K. Fujimoto, T. Yonezawa, E. Wachi, Y. Yamaguchi, M. Nakano, R.P. Shogan, J.-P. Massoud, T.R. Mager, in: 12th International Conference on Environmental Degradation of Materials in nuclear Power System, 2005.
[42] K. Fujii, K. Fukuya, G. Furutani, T. Torimaru, A. Kohyama, Y. Katoh, in: 10th International Conference on Environmental Degradation of Materials in nuclear Power System, 2002.
[43] J.R. Rice, J.S. Wang, Mater. Sci. Eng. A 107 (1989) 23.
[44] W.T. Geng, A.J. Freeman, R. Wu, C.B. Geller, J.E. Raynolds, Phys. Rev. B 60 (10) (1999) 7149.
[45] G.A. Young, R. Najafabadi, W. Strohmayer, D.G. Baldrey, W.L. Hamm, in: 11th International Conference on Environmental Degradation of Materials in Nuclear Power System, 2003.
[46] M. Yamaguchi, M. Shiga, H. Kaburaki, J. Phys.: Condens. Matter 16 (2004) 3933.
[47] A. Van der Ven, G. Ceder, Acta Mater. 52 (2004) 1223.
[48] D.E. Jiang, E.A. Carter, Acta Mater. 52 (2004) 4801.
[49] E.D. Hondros, M.P. Seah, Metall. Trans. A Phys. Metall. Mater. Sci. 8 (9) (1977) 1363.
[50] J.P. Hirth, Metall. Trans. A 11A (1980) 861.
[51] J. Chêne, EDP Sciences, PlastOx, 2009, pp. 131.
[52] K. Asano, K. Fukuya, K. Nakata, M. Kodoma, in: 5th International Conference on Environmental Degradation of Materials in Nuclear Power System, 1992.
[53] Y. Miwa, Y. Kaji, N. Okubo, K. Kondo, T. Tsukada, J. Solid Mech. Mater. Eng. 2 (2008) 145.
[54] S.M. Bruemmer, L.E. Thomas, in: 12th International Conference on Environmental Degradation of Materials in Nuclear Power System, 2005.
[55] C.A.J. Fisher, Scripta Mater. 50 (2004) 1045.
[56] J. Sun, T. Stirmer, A. Matthews, Surf. Coat. Technol. 201 (2006) 4205.
[57] N.H. de Leeuw, T.G. Cooper, Geochim. Cosmochim. Acta. 71 (2007) 1655.
[58] D.J. Edwards, F.A. Garner, S.M. Bruemmer, P. Efsing, J. Nucl. Mater. 384 (2009) 249.
[59] T. Diaz de la Rubia, H.M. Zbib, T.A. Khralshl, B.D. Wirth, M. Victoria, M.J. Caturia, Lett. Nat. 406 (2000) 871.
[60] N.M. Ghoniem, S.-H. Tong, B.N. Singh, L.Z. Sun, Philos. Mag. A 81 (2001) 2743.
[61] J.S. Robach, I.M. Robertson, B.D. Wirth, A. Arsenlis, Philos. Mag. 83 (2003) 955.
[62] Y.T. Chou, J.C.M. Li, in: T. Mura (Ed.), Mathematical Theory of Dislocations, ASME, New-York, 1969, p. 116.
[63] F.W. Young, J. Appl. Phys. 33 (1962) 3553.
[64] D.L. Mc Dowell, Mater. Sci. Eng. Res. 62 (2008) 67.
[65] T.C. Lee, I.M. Robertson, H.K. Birnbaum, Scripta Metal 23 (1989) 799.
[66] J.V. Sharp, Philos. Mag. 16 (1976) 77.
[67] N.J. Wadsworth, J. Hutchings, Philos. Mag. 8 (1964) 195.
[68] P.O. Kettunen, Acta Metal 15 (1967) 1275.
[69] J. Dehrs, J. Driver, International Colloquium on Basic Mechanisms in Fatigue of Metals, Academia, Prague, 1988.
[70] N. Hansen, X. Huang, Acta Mater. 46 (1998) 1827.
[71] M. Sauzay, Th. Jourdan, Int. J. Fatigue 141 (2006) 431.
[72] M. Sauzay, Acta Mater. 55 (2007) 1193.
[73] M. Sauzay, in: International Conference on Fracture, Ottawa, 2009.
[74] U. Lienert, T.-S. Han, J. Almer, P.R. Dawson, T. Leffers, L. Margulies, S.F. Nielsen, H.F. Poulsen, S. Schmidt, Acta Mater. 52 (2004) 4461.
[75] S. Osterstock, Ch. Robertson, M. Sauzay, S. Degallaix, V. Aubin, Key Eng. Mater. 345–346 (2007) 363.